RSC Sustainability

ROYAL SOCIETY OF CHEMISTRY

COMMUNICATION

View Article Online
View Journal | View Issue

Cite this: *RSC Sustainability*, 2026, **4**, 748

Received 13th November 2025
Accepted 18th December 2025

DOI: 10.1039/d5su00861a

rsc.li/rscsus

A tandem approach for waste-to-nanomaterial transformation towards polyethylene recycling

Yanan Huang,[a] Chi-Linh Do-Thanh,[b] Zhenzhen Yang,*[c] Sheng Dai*[bc] and Hao Chen*[ab]

Polyethylene (PE) waste was recycled into nanoporous carbon materials *via* $NaNH_2$-catalyzed tandem cross-linking and carbonization. The process enables C–H cleavage and C–N formation, yielding carbons with surface areas up to 2080 $m^2\ g^{-1}$. The resulting materials exhibit excellent performance in gas separation and energy storage applications.

The overconsumption of single-use plastics, which have long lifetimes, slow decomposition rates, and the potential to disrupt ecosystems, has raised widespread environmental, economic, and health concerns.[1–3] Compared to mechanical recycling, landfilling, and incineration, the selective conversion of single-use plastics in the presence of heterogeneous, homogeneous, or biocatalytic systems represents a promising research direction. This approach enables the recycling of waste into value-added chemicals (building blocks), advanced materials (carbons), and fuels (liquid hydrocarbons), deploying polyethylene (PE), polypropylene (PP), polyethylene terephthalate (PET), polyurethane (PU), polyvinyl chloride (PVC), or polystyrene (PS) as starting materials.[3,4] For example, *via* pyrolysis, PE recycling in the presence of $CuCO_3$ (ref. 5) or PP recycling in the presence of zeolites (*e.g.*, HY-2.8 or NaY-2.8) could generate liquid hydrocarbons.[6,7] Heterogeneous metal nanocatalysts capable of activating H_2 have been demonstrated for the hydrocracking of PE (*e.g.*, $Pt/SiTiO_3$ or SiO_2/Pt)[8,9] or mixed plastic waste (*e.g.*, Al-SBA-15)[10] to generate motor oil or liquid hydrocarbons. The dehydrochlorination of PVC[11] or glycolysis of PET[12,13] could produce the corresponding monomers. Besides these approaches for obtaining small-molecule chemicals or liquid products, the gasification–carbonization of PP, PE, or PET could also form carbonaceous nanomaterials.

Sustainability spotlight

The excessive use of single-use plastics, due to their persistence and slow degradation, has generated significant environmental, economic, and health concerns. In this work, we developed a tandem cross-linking/carbonization route for converting polyethylene (PE) into advanced carbon materials. Subsequent carbonization yields high-quality nanoporous carbons with surface areas of up to 2080 $m^2\ g^{-1}$, outperforming previous plastic-to-carbon methods. The resulting materials exhibit excellent performance in gas separation and energy storage.

In the presence of organically modified montmorillonite-based catalytic systems (no additives or doping with Co_3O_4 or NiO), plastic recycling could be achieved to generate graphene flakes, hollow carbon spheres, or multi-walled carbon nanotubes (MWCNTs).[14–17] The carbonization of mixed plastic waste catalyzed by Ni/Al_2O_3 led to the formation of CNTs.[18] Heterostructures composed of carbon and metal oxides (*e.g.*, Fe_3O_4@C core–shell structures) were obtained from PE in the presence of ferrocene and ammonium carbonate.[19,20] Although progress has been made, the utilization of plastic waste to produce high-quality carbon materials is still highly underexplored. In particular, high catalyst loading (up to 800 wt%), the requirement for metal additives, and the inferior porosity of the carbonaceous products have restricted the application of plastic-to-carbon strategies in energy-related fields. Particularly, compared with PET, PU, and PVC containing extra ester, urea, or halide moieties, high- and low-density polyethylene (HDPE and LDPE), and PP solely composed of strong single C–C and C–H bonds within the plastic skeleton have exhibited higher thermodynamic stability and kinetic inertness, leading to energy-intensive and low-efficiency recycling outcomes even under rigorous conditions.[1] Facile approaches capable of producing high-quality nanoporous carbons deploying PE-based starting materials will represent a critical development for cost-effective and high-performance plastic-to-material pathways towards energy-related applications.

[a]*State Key Laboratory for Chemo and Biosensing, College of Chemistry and Chemical Engineering, Hunan University, Changsha, 410082, China. E-mail: dais@ornl.gov*
[b]*Department of Chemistry, Institute for Advanced Materials and Manufacturing, University of Tennessee, Knoxville, TN 37996, USA*
[c]*Chemical Sciences Division, Oak Ridge National Laboratory, Oak Ridge, TN 37831, USA. E-mail: yangz3@ornl.gov*

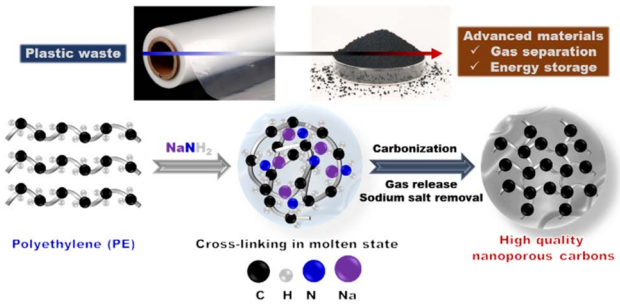

Fig. 1 A schematic illustration of PE recycling by $NaNH_2$-promoted cross-linking/carbonization to produce advanced materials.

Herein, a tandem cross-linking and carbonization pathway was developed towards the transformation of PE to advanced materials (Fig. 1). Sodium amide ($NaNH_2$), with its strong basicity and nucleophilic activity, was deployed as the catalyst for C–H bond cleavage in the PE skeleton and new C–N bond construction, leading to cross-linking of the PE precursor and enhanced thermal stability, which was then followed by carbonization *via* thermal treatment into high-quality nanoporous carbon materials with surface areas up to 2080 $m^2\ g^{-1}$, surpassing those obtained *via* previously demonstrated procedures for plastic waste carbonization. The high surface area and abundant micropores within the carbon skeletons gave the afforded materials impressive performance in CO_2 capture/separation and energy storage as a component in supercapacitor construction. This study provides new insight into PE recycling to afford promising material candidates for energy-related fields.

Screening of the reaction parameters was conducted using the surface area of the carbon products as an indicator, which is an important feature in the fields of gas uptake, catalysis, and energy storage. PE with a molecular weight of 3000 was used as the precursor. It was pyrolyzed from 410 to 480 °C (Fig. S1A) and exhibited a sphere-like morphology (Fig. S1B). Using $NaNH_2$ as the catalyst, different carbon materials are fabricated by varying the catalyst loading and reaction temperature. The as-prepared carbon materials are denoted as C-*m*-*T* (*m* = mass ratio of $NaNH_2$: PE, *T* = reaction temperature). The Brunauer–Emmett–Teller (BET) surface areas of the products are analysed by N_2 absorption at 77 K (Fig. 2A, S1C, S2 and S3). The N_2 adsorption–desorption isotherms of the PE precursor show a nearly featureless profile with extremely low adsorption capacity, indicating its non-porous or very weakly porous nature. With a reaction temperature of 850 °C, C-0.1-850 obtained with a $NaNH_2$: PE mass ratio of 0.1 showed a surface area of 703 $m^2\ g^{-1}$; increasing the loading amount of $NaNH_2$ led to an enhanced surface area, with C-0.25-850 exhibiting a surface area of 1450 $m^2\ g^{-1}$. However, further increasing the $NaNH_2$: PE mass ratio had an inferior effect on the surface areas of the carbon products, leading to the formation of C-0.5-850 and C-0.75-850 with surface areas of 1033 and 630 $m^2\ g^{-1}$, respectively. These results indicated that a $NaNH_2$: PE mass ratio of 0.25 is optimal to generate carbon materials with high surface areas. The creation of porosity in the carbon skeleton was

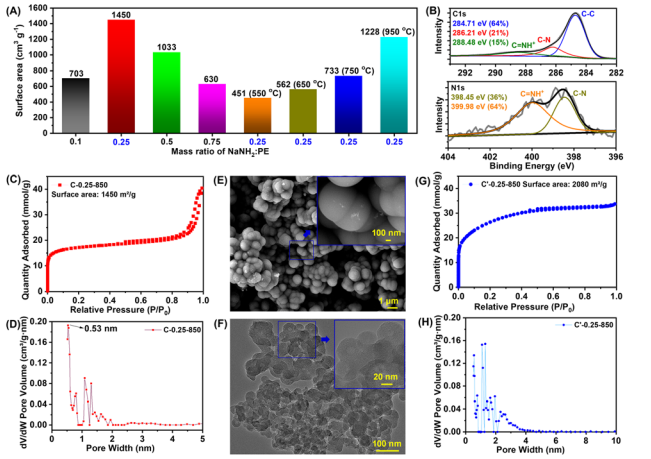

Fig. 2 (A) The surface areas of the carbon materials obtained with different mass ratios of $NaNH_2$:PE and reaction temperatures. (B) C 1s and N 1s XPS spectra, (C) N_2 sorption and desorption isotherms (77 K), (D) the pore size distribution curve, and (E) SEM and (F) TEM images of C-0.25-850. (G) N_2 sorption and desorption isotherms and (H) the pore size distribution curve of C′-0.25-850.

possibly due to gas formation and release (*e.g.*, H_2, CH_4, and NH_3) upon C–C bond construction during the reaction procedure in the presence of $NaNH_2$.[21] The diminished surface areas of carbons in the presence of high loading amounts of $NaNH_2$ was probably owing to the collapse of nanoporous structures driven by the strong basicity of the amide anions and the partial decomposition of carbon moieties. Examining the Raman spectra (Fig. S4), two characteristic bands centered at ~1350 and ~1580 cm^{-1}, corresponding to the D and G bands of carbonaceous species, are clearly observed for C-0.1-850. The prominent D and G signals indicate the presence of defect-rich sp^2 carbon domains formed during the thermal treatment.[22] As the mass ratio of $NaNH_2$: PE increased, the intensities of both bands decreased significantly, suggesting the formation of more disordered carbon structures. TGA results indicate that an appropriate amount of $NaNH_2$ enhances the thermal stability of the carbon materials, whereas excessive $NaNH_2$ loading leads to a decrease in thermal stability (Fig. S5). Subsequently, the influence of reaction temperature was studied using a $NaNH_2$: PE mass ratio of 0.25 in the range of 550–950 °C. The successful carbonization of PE was achieved at a reaction temperature of 550 °C with a carbon yield of 25%, generating C-0.25-550 with a surface area of 451 $m^2\ g^{-1}$. Increasing the reaction temperature to 650 and 750 °C only showed slight improvements in the porosity of the carbon products, with C-0.25-650 (carbon yield: 28%) and C-0.25-750 (carbon yield: 30%) having surface areas of 562 and 733 $m^2\ g^{-1}$, respectively. Comparatively, C-0.25-850 synthesized at 850 °C, exhibited a significantly increased surface area (1450 $m^2\ g^{-1}$). However, further increasing the reaction temperature to 950 °C resulted in a slight decrease in the surface area of C-0.25-950 (1228 $m^2\ g^{-1}$) and its carbon yield (20%).

Detailed characterization of C-0.25-850 with the highest surface area was conducted to determine more structural information. The powder X-ray diffraction (PXRD) pattern of the

PE precursor exhibited a crystalline structure, which, upon cross-linking and decomposition in the presence of $NaNH_2$ and at high temperature, became an amorphous carbon product (C-0.25-850) (Fig. S6). A comparison of the Fourier-transform infrared (FTIR) spectra indicated the complete loss of the aliphatic C–H moieties within the skeleton of C-0.25-850, which were clearly seen at around 2900 cm^{-1} in the PE precursor (Fig. S7), demonstrating the high catalytic efficiency of $NaNH_2$ in the cleavage of the C–H bonds during the thermal treatment procedure. X-ray photoelectron spectroscopy (XPS) analysis showed that C-0.25-850 was composed of carbon and nitrogen, with the latter only occupying 0.8 at% on the surface. Therefore, most of the nitrogen moieties were released in the form of gaseous products *via* decomposition at high temperature. The C 1s spectrum of C-0.25-850 could be deconvoluted into three major peaks with binding energies (BEs) of 284.71, 286.21, and 288.48 eV, corresponding to the carbon atoms in C–C, C–N, and C=NH^+, respectively (Fig. 2B).[23] This is in accordance with the N 1s spectrum, with two major peaks at BEs of 398.45 (C–N) and 399.98 eV (C=NH^+). The N_2 adsorption and desorption isotherms of C-0.25-850 showed a type-I reversible profile (Fig. 2C), which exhibited steep N_2 sorption in the low-pressure region (<0.01 bar) derived from the existence of micropores. Pore size distribution curves calculated by the nonlocal density functional theory (NLDFT) method demonstrated the presence of micropores of around 0.53 and 1.0–2.0 nm (Fig. 2D). The total surface area (1450 $m^2\ g^{-1}$) was dominated by the micropore area (1051 $m^2\ g^{-1}$), with a small amount of external surface area (399 $m^2\ g^{-1}$). Correspondingly, the total pore volume of 0.93 $cm^3\ g^{-1}$ comprised 0.42 $cm^3\ g^{-1}$ from micropores. Scanning electron microscopy (SEM) showed that C-0.25-850 was composed of particles with sphere-like morphology and a smooth surface structure (Fig. 2E). Transmission electron microscopy (TEM) images further confirm the sphere-like particles, with some of them containing hollow spaces and the existence of porous structures (Fig. 2F). With the achievements made using PE with a molecular weight of 3000 as the precursor, the $NaNH_2$-promoted carbonization procedure was further extended to PE with a high molecular weight (35 000). With a $NaNH_2$: PE_{35000} mass ratio of 0.25 and reaction temperature of 850 °C, the afforded carbon material was denoted as C′-0.25-850; it had amorphous morphology, as indicated by the PXRD pattern (Fig. S8), and showed no characteristic signals for C–H bonds in the FTIR spectrum (Fig. S9). Porosity analysis by N_2 sorption isotherms revealed that C′ −0.25 −850 had an improved surface area (2080 $m^2\ g^{-1}$) compared with the carbon product from PE_{3000} under the same conditions (Fig. 2G), with 551 $m^2\ g^{-1}$ derived from the micropore area and 1529 $m^2\ g^{-1}$ from the external surface area. The total pore volume was 1.14 $cm^3\ g^{-1}$, with 0.25 $cm^3\ g^{-1}$ contributed by micropores. The pore size distribution curve calculated from the NLDFT method exhibited the co-existence of micropores (<2 nm) and mesopores (2–4 nm) (Fig. 2H). All the above-mentioned results demonstrated the high catalytic activity of $NaNH_2$ for the activation and cleavage of the C–H bonds in PE and the formation of C–C bonds in the construction of carbon skeletons. Specifically, $NaNH_2$ acts as a strong nucleophilic species that can initiate C–H bond activation in PE *via* deprotonation-driven cleavage.[24] This process generates highly reactive carbon-centered intermediates, which subsequently undergo dehydrogenation and radical-like cross-linking reactions, thereby accelerating the formation of a more interconnected carbon framework.[25] With only a catalytic amount of catalyst and without other templates or additives, high-quality nanoporous carbon materials could be afforded with surface areas surpassing PE-derived carbon materials generated by other methodologies (Table S1), most polymer-derived carbons using hard/soft templates[26] and even carbon materials activated by excess amounts of $NaNH_2$ (*e.g.*, 2 equivalents).[25]

Carbonaceous materials have shown wide applications in the fields of gas storage and separation, catalysis, and energy storage.[26,27] CO_2 capture and sequestration (CCS) represents one of the most intensively studied technologies towards alleviating the global greenhouse gas impact.[28–32] Nanomaterials with high surface areas and the involvement of micro- or ultra-micropores are preferred, as they are capable of achieving high CO_2 uptake capacities and selectivities.[33,34] The as-prepared carbon materials from PE recycling exhibited high surface areas up to 2080 $m^2\ g^{-1}$ and abundant micropores within the skeleton, which made them promising candidates for CO_2 capture and separation. The CO_2 uptake isotherms of the nanoporous carbon materials are collected at 273 and 29 K (Table S2, Fig. 3A and B), among which C −0.25 −850 exhibited the highest CO_2 uptake capacity. As shown in Fig. 3A, the CO_2 uptake capacities of C −0.25 −850 reached 5.31 and 3.32 mmol g^{-1} at 273 and 298 K, respectively, which were higher than most of the carbon-based materials reported in the literature[35–39] and are comparable to the capacities of nitrogen-doped systems (Table S2).[40–42] The CO_2/N_2 selectivities were calculated to be 27 and 24 at 273 and 298 K, respectively, by the ideal adsorption solution theory (IAST) with a ratio of N_2 : CO_2 of 85 : 15. The isosteric heat of adsorption (Q_{st}) was calculated to be 27.8 kJ mol^{-1} for C-0.25-850 (Fig. 3C). Comparatively, the CO_2 uptake capacities of C′-0.25-850 with a higher surface area (2080 $m^2\ g^{-1}$) did not surpass those obtained by C-0.25-850 (5.21 mmol g^{-1} at 273 K and 1 bar; 3.53 mmol g^{-1} at 298 K and 1 bar) because C −0.25 −850 contained a larger fraction of micropores (especially pores <0.7 nm), which exhibit stronger affinity toward CO_2 molecules (kinetic diameter ≈0.33 nm)[43] and therefore deliver higher uptakes at low pressures. In contrast, although C′-0.25-850 possesses a higher BET surface area than C-0.25-850, its adsorption in the low-pressure region is much less pronounced (Fig. 2G), suggesting that the additional surface area mainly originates from mesopores/macropores or pore structures that

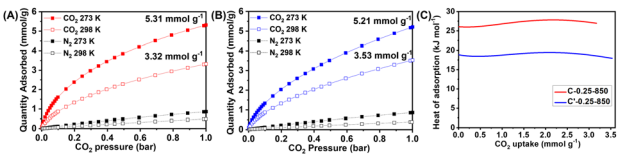

Fig. 3 (A) CO_2 and N_2 isotherms of C-0.25-850 at 273 and 298 K. (B) CO_2 and N_2 isotherms of C′-0.25-850 at 273 and 298 K. (C) Heats of adsorption of C-0.25-850 and C′-0.25-850 in CO_2 capture.

are unfavorable for strong CO_2 adsorption. The CO_2/N_2 selectivities of C′-0.25-850 were calculated to be 41 and 30, respectively, together with a Q_{st} value of 19.5 kJ mol^{-1}. The CO_2 capture results demonstrated that *via* the $NaNH_2$-promoted cross-linking and carbonization procedure, stable plastic waste is transformed into advanced materials that are good adsorbents for CO_2 capture and separation.

The high surface areas and abundant porosity of the afforded carbon materials prompted us to further explore their applications in energy storage. Among diverse devices, supercapacitors, featuring high power densities, good reversibility, wide operating temperatures, and long cycle lives, have attracted extensive attention, being deployed as critical components in frequency modulators, tube voltage-stabilizers, consumer electronics, and hybrid electric vehicles.[44–47] Supercapacitors can be categorized into electrical double-layer capacitors (EDLCs) and pseudocapacitors, in which the charge storage mechanism occurs *via* physical electrostatic adsorption and reversible surface chemical redox reactions, respectively.[48] EDLCs generally display enhanced power densities, improved stability in extreme heat or cold, and prolonged cycling lives compared with pseudocapacitors. Material skeletons composed of sp^2 carbons, featuring high surface areas, appropriate pore size distributions, good conductivity, and excellent chemical stability, are preferred as promising electrode materials in EDLCs.[49,50] The unique features of the nanoporous carbon materials generated from PE recycling in this work enable them to be promising candidates for use in supercapacitors. The capacitive behaviors were evaluated in a three-electrode system using 1 M aqueous H_2SO_4 electrolyte with an Ag/AgCl reference electrode and a platinum counter electrode. Taking C-0.25-750 with a surface area of 733 m^2 g^{-1} as an example, all the collected cyclic voltammetry (CV) curves at different scan rates of 5–500 mV s^{-1} exhibited symmetric rectangular shapes with weakly broadened humps appearing at potentials of 0–0.6 V (Fig. 4A), demonstrating a combination of EDLC and pseudocapacitance.[51] Then, PE-derived carbon materials (with a mass ratio of 0.25 for $NaNH_2$:PE) generated under various conditions were evaluated at 50 mV s^{-1} (Fig. 4B). The hump increased from C-0.25-550 to C-0.25-750 and then diminished in C-0.25-850 and C-0.25-950, with the maximum value being achieved by C-0.25-750, probably owing to the decreased numbers of heteroatoms within the skeleton at higher temperatures. These heteroatoms provide additional pseudocapacitance and improve electrode wettability, which outweighs the effects of surface area alone. With higher temperature (850–950 °C) treatment, the content of heteroatoms in carbon materials decreases significantly, leading to a reduced pseudocapacitive contribution despite the larger BET surface area.[52,53] The electrochemical impedance spectroscopy (EIS) measurement results show a clear decrease in charge-transfer resistance upon increasing the activation temperature from 550 to 750 °C, and it then increased as the activation temperature increased from 750 to 950 °C. This trend is fully consistent with the capacitance measurements, where samples with higher porosity and conductivity exhibit superior electrochemical performance (Fig. S10). Correspondingly, the optimal capacitance values were obtained by C-0.25-750, which were calculated to be 212.2 and 141.9 F g^{-1} at scan rates of 5 and 500 mV s^{-1}, respectively, with 67% retention at the higher scan rate (Fig. 4C). The long-term cycling performance was evaluated using C-0.25-750 by chronopotentiometric charge/discharge tests. Capacitance retention of 88.6% for more than 5000 cycles (Fig. 4D) was maintained at a high constant current density of 5 A g^{-1}. All these results demonstrated that when using single-use plastic waste as a raw material, the facile $NaNH_2$-promoted carbonization pathway led to the generation of high-quality carbon materials that can act as promising components in the field of energy storage.

In conclusion, by deploying a suitable catalyst, a PE precursor can be easily decomposed under an inert atmosphere and transformed into nanoporous carbon materials. The key lies in the cross-linking of the PE chains first to improve the thermal stability, followed by the generation of the nanoporous materials *via* high-temperature thermal treatment. This facile strategy allows the successful transformation of discarded plastics into advanced materials with good performance in gas separation and energy storage.

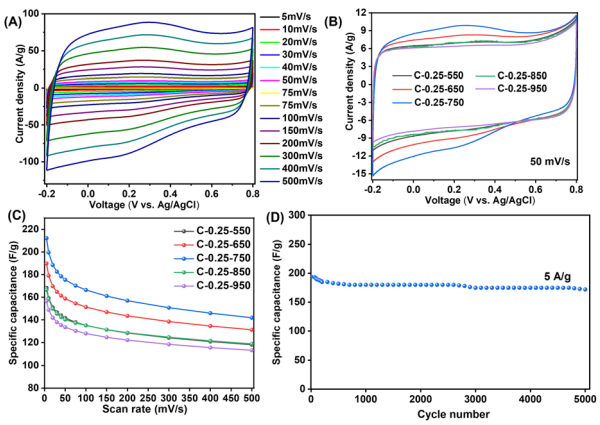

Fig. 4 (A) CV curves of C-0.25-750 at different scan rates from 5 to 500 mV s^{-1}. (B) CV curves of C-0.25-*T* (*T* = heating temperature) at 50 mV s^{-1}. (C) CV rate performances of C-0.25-*T*. (D) The GCD long-term cycling performance of C-0.25-750 at 5 A g^{-1}.

Author contributions

Yanan Huang: conceptualization, methodology, software, data curation, writing – original draft. Chi-Linh Do-Thanh: software, data curation, writing – review & editing. Zhenzhen Yang: funding acquisition, project administration, writing – review & editing. Hao Chen: supervision, funding acquisition, project administration, writing – review & editing. Sheng Dai: supervision, funding acquisition, project administration, writing – review & editing. All authors discussed the results and commented on the manuscript.

Conflicts of interest

There are no conflicts to declare.

Data availability

All data supporting the findings of this study are available within the article and its supplementary information (SI) file. Supplementary information is available including the detailed information of materials, characterizations and methods in this work, as well as the supplementary results of XRD, TGA, SEM, Raman, FTIR and N_2 adsorption-desorption. See DOI: https://doi.org/10.1039/d5su00861a.

Acknowledgements

H. C. was supported by the National Key R&D Program of China (2023YFB4103000).

Notes and references

1 A. J. Martín, C. Mondelli, S. D. Jaydev and J. Pérez-Ramírez, *Chem*, 2021, **7**(6), 1487–1533.
2 J. R. Jambeck, R. Geyer, C. Wilcox, T. R. Siegler, M. Perryman, A. Andrady, R. Narayan and K. L. Law, *Science*, 2015, **347**(6223), 768.
3 M. Haussler, M. Eck, D. Rothauer and S. Mecking, *Nature*, 2021, **590**(7846), 423–427.
4 X. Jiao, K. Zheng, Z. Hu, S. Zhu, Y. Sun and Y. Xie, *Adv. Mater.*, 2021, e2005192.
5 M. V. Singh, S. Kumar and M. Sarker, *Sustainable Energy Fuels*, 2018, **2**(5), 1057–1068.
6 W. Zhao, S. Hasegawa, J. Fujita, F. Yoshii, T. Sasaki, K. Makuuchi, J. Sun and S.-i. Nishimoto, *Polym. Degrad. Stab.*, 1996, **53**(1), 129–135.
7 M. Blazsó, *J. Anal. Appl. Pyrolysis*, 2005, **74**(1), 344–352.
8 G. Celik, R. M. Kennedy, R. A. Hackler, M. Ferrandon, A. Tennakoon, S. Patnaik, A. M. LaPointe, S. C. Ammal, A. Heyden, F. A. Perras, *et al.*, *ACS Cent. Sci.*, 2019, **5**(11), 1795–1803.
9 A. Tennakoon, X. Wu, A. L. Paterson, S. Patnaik, Y. Pei, A. M. LaPointe, S. C. Ammal, R. A. Hackler, A. Heyden, I. I. Slowing, *et al.*, *Nat. Catal.*, 2020, **3**(11), 893–901.
10 D. Munir, F. Piepenbreier and M. R. Usman, *Powder Technol.*, 2017, **316**, 542–550.
11 A. Seino, T. Nishizaki, Y. Kanda, M. Sugioka and Y. Uemichi, *J. Jpn. Pet. Inst.*, 2009, **52**(2), 70–71.
12 M. Imran, D. H. Kim, W. A. Al-Masry, A. Mahmood, A. Hassan, S. Haider and S. M. Ramay, *Polym. Degrad. Stab.*, 2013, **98**(4), 904–915.
13 F. R. Veregue, C. T. Pereira da Silva, M. P. Moisés, J. G. Meneguin, M. R. Guilherme, P. A. Arroyo, S. L. Favaro, E. Radovanovic, E. M. Girotto and A. W. Rinaldi, *ACS Sustainable Chem. Eng.*, 2018, **6**(9), 12017–12024.
14 T. Tang, X. Chen, X. Meng, H. Chen and Y. Ding, *Angew. Chem., Int. Ed.*, 2005, **44**(10), 1517–1520.
15 J. Gong, J. Liu, X. Wen, Z. Jiang, X. Chen, E. Mijowska and T. Tang, *Ind. Eng. Chem. Res.*, 2014, **53**(11), 4173–4181.
16 J. Gong, J. Liu, Z. Jiang, X. Chen, X. Wen, E. Mijowska and T. Tang, *Appl. Catal., B*, 2014, **152–153**, 289–299.
17 Y. Yuan, Z. Xie, K. K. Turaczy, S. Hwang, J. Zhou and J. G. Chen, *Chem Bio Eng.*, 2024, **1**(1), 67–75.
18 R.-X. Yang, K.-H. Chuang and M.-Y. Wey, *Energy Fuels*, 2015, **29**(12), 8178–8187.
19 J. Zhang, B. Yan, S. Wan and Q. Kong, *Ind. Eng. Chem. Res.*, 2013, **52**(16), 5708–5712.
20 N. A. Elessawy, E. M. El-Sayed, S. Ali, M. F. Elkady, M. Elnouby and H. A. Hamad, *J. Water Process. Eng.*, 2020, **34**, 101047.
21 J. Wang and S. Kaskel, *J. Mater. Chem.*, 2012, **22**(45), 23710–23725.
22 S. I. Moseenkov, V. L. Kuznetsov, N. A. Zolotarev, B. A. Kolesov, I. P. Prosvirin, A. V. Ishchenko and A. V. Zavorin, *Materials*, 2023, **16**(3), 1112.
23 Z. Yang, T. Wang, H. Chen, X. Suo, P. Halstenberg, H. Lyu, W. Jiang, S. M. Mahurin, I. Popovs and S. Dai, *ACS Energy Lett.*, 2020, **6**(1), 41–51.
24 R. A. Woltornist, Y. Ma, R. F. Algera, Y. Zhou, Z. Zhang and D. B. Collum, *Synthesis*, 2020, **52**(10), 1478–1497.
25 K. Huang, S.-H. Chai, R. T. Mayes, S. Tan, C. W. Jones and S. Dai, *Microporous Mesoporous Mater.*, 2016, **230**, 100–108.
26 H. Wang, Y. Shao, S. Mei, Y. Lu, M. Zhang, J. K. Sun, K. Matyjaszewski, M. Antonietti and J. Yuan, *Chem. Rev.*, 2020, **120**(17), 9363–9419.
27 M. R. Benzigar, S. N. Talapaneni, S. Joseph, K. Ramadass, G. Singh, J. Scaranto, U. Ravon, K. Al-Bahily and A. Vinu, *Chem. Soc. Rev.*, 2018, **47**(8), 2680–2721.
28 S. J. Datta, C. Khumnoon, Z. H. Lee, W. K. Moon, S. Docao, T. H. Nguyen, I. C. Hwang, D. Moon, P. Oleynikov, O. Terasaki, *et al.*, *Science*, 2015, **350**(6258), 302–306.
29 R. Monastersky, *Nature*, 2013, **497**, 13.
30 S. Zeng, X. Zhang, L. Bai, X. Zhang, H. Wang, J. Wang, D. Bao, M. Li, X. Liu and S. Zhang, *Chem. Rev.*, 2017, **117**(14), 9625–9673.
31 K. Sumida, D. L. Rogow, J. A. Mason, T. M. McDonald, E. D. Bloch, Z. R. Herm, T.-H. Bae and J. R. Long, *Chem. Rev.*, 2011, **112**(2), 724–781.
32 A. S. Palakkal, S. A. Mohamed and J. Jiang, *Chem Bio Eng.*, 2024, **1**(11), 970–978.
33 W. Gao, S. Liang, R. Wang, Q. Jiang, Y. Zhang, Q. Zheng, B. Xie, C. Y. Toe, X. Zhu, J. Wang, *et al.*, *Chem. Soc. Rev.*, 2020, **49**(23), 8584–8686.
34 A. E. Creamer and B. Gao, *Environ. Sci. Technol.*, 2016, **50**(14), 7276–7289.
35 K. Huang, S.-H. Chai, R. T. Mayes, G. M. Veith, K. L. Browning, M. A. Sakwa-Novak, M. E. Potter, C. W. Jones, Y.-T. Wu and S. Dai, *Chem. Commun.*, 2015, **51**(97), 17261–17264.
36 P. Puthiaraj, Y.-R. Lee and W.-S. Ahn, *Chem. Eng. J.*, 2017, **319**, 65–74.
37 N. A. Rashidi and S. Yusup, *J. Cleaner Prod.*, 2017, **168**, 474–486.
38 N. S. Nasri, U. D. Hamza, S. N. Ismail, M. M. Ahmed and R. Mohsin, *J. Cleaner Prod.*, 2014, **71**, 148–157.
39 L. Wang and R. T. Yang, *J. Phys. Chem. C*, 2012, **116**(1), 1099–1106.

40 Y. Boyjoo, Y. Cheng, H. Zhong, H. Tian, J. Pan, V. K. Pareek, J.-F. Lamonier, M. Jaroniec and J. Liu, *Carbon*, 2017, **116**, 490–499.
41 L. Yue, Q. Xia, L. Wang, L. Wang, H. DaCosta, J. Yang and X. Hu, *J. Colloid Interface Sci.*, 2018, **511**, 259–267.
42 L. Yue, L. Rao, L. Wang, L. An, C. Hou, C. Ma, H. DaCosta and X. Hu, *Energy Fuels*, 2018, **32**(6), 6955–6963.
43 Y. S. Bae and R. Q. Snurr, *Angew Chem. Int. Ed. Engl.*, 2011, **50**(49), 11586–11596.
44 J. R. Miller and P. Simon, *Science*, 2008, **321**(5889), 651.
45 D. Kong, Y. Gao, Z. Xiao, X. Xu, X. Li and L. Zhi, *Adv. Mater.*, 2019, **31**(45), e1804973.
46 W. Raza, F. Ali, N. Raza, Y. Luo, K.-H. Kim, J. Yang, S. Kumar, A. Mehmood and E. E. Kwon, *Nano Energy*, 2018, **52**, 441–473.
47 H. Chen, Z. Yang, W. Guo, J. R. Dunlap, J. Liang, Y. Sun, K. Jie, S. Wang, J. Fu and S. Dai, *Adv. Funct. Mater.*, 2019, **29**(50), 1906284.
48 L. L. Zhang and X. Zhao, *Chem. Soc. Rev.*, 2009, **38**(9), 2520–2531.
49 L. Zhang, X. Yang, F. Zhang, G. Long, T. Zhang, K. Leng, Y. Zhang, Y. Huang, Y. Ma and M. Zhang, *J. Am. Chem. Soc.*, 2013, **135**(15), 5921–5929.
50 R. Dash, J. Chmiola, G. Yushin, Y. Gogotsi, G. Laudisio, J. Singer, J. Fischer and S. Kucheyev, *Carbon*, 2006, **44**(12), 2489–2497.
51 K. Wang, N. Zhao, S. Lei, R. Yan, X. Tian, J. Wang, Y. Song, D. Xu, Q. Guo and L. Liu, *Electrochim. Acta*, 2015, **166**, 1–11.
52 K. Huang, S. H. Chai, R. T. Mayes, G. M. Veith, K. L. Browning, M. A. Sakwa-Novak, M. E. Potter, C. W. Jones, Y. T. Wu and S. Dai, *Chem.Commun.*, 2015, **51**(97), 17261–17264.
53 H. M. Jeong, J. W. Lee, W. H. Shin, Y. J. Choi, H. J. Shin, J. K. Kang and J. W. Choi, *Nano Lett.*, 2011, **11**(6), 2472–2477.